Supporting Information

Integration of Confinement Crosslinking and In-Situ Grafting for Constructing Artificial Interphase toward Stabilized Zinc Anodes

Feng Zhang[a], Jia-Wei Qian[a], Wei-Xu Dong[a], Yi-Fan Qu[a], Kai Chen[a], Jingwei Chen[b,*], Yang-Feng Cui[c], Li-Feng Chen[a,*]

[a]Division of Nanomaterials & Chemistry, Hefei National Research Center for Physical Sciences at the Microscale, School of Chemistry and Materials Science, CAS Key Laboratory of Mechanical Behavior and Design of Materials (LMBD), School of Engineering Science, University of Science and Technology of China, Hefei 230026, Anhui, China.
[b]School of Materials Science and Engineering, Ocean University of China, Qingdao 266100, China.
[c]Pillar of Engineering Product Development, Singapore University of Technology and Design, Singapore, 487372 Singapore.

[*]Corresponding author. E-mail: chenlf@ustc.edu.cn (Li-Feng Chen); chenjingwei@ouc.edu.cn (Jingwei Chen).

Experimental section

Synthesis of hollow SSZ13 molecular sieve

The hollow SSZ13 molecular sieves were prepared according to a previous report.[S1] Firstly, 0.2 g of $NaAlO_2$ were uniformly dispersed in 18.0 g of deionized H_2O, and then about 0.8 g of N,N,N-trimethyl-1-adamantylammonium hydroxide (TMAdaOH) were added into the aforementioned solution, which was stirred for 1 h. Secondly, 0.1 g of NaOH and 8.0 g of 30 % silica gels were simultaneously mixed with the above solution, stirring for another 3 h. Thirdly, the obtained solution was transferred to a teflon-lined stainless-steel autoclave, which was subjected to a hydrothermal reaction at 160 °C in a rotating oven for 72 h. Fourthly, the acquired white suspension was centrifugally washed with deionized H_2O for three times, and the white solid materials were dried at 80 °C for 12 h. Fifthly, the above dried samples were calcined in a muffle oven at 600 °C for 12 h with a heating rate of 1 °C min^{-1}, obtaining the white products of solid SSZ13 molecular sieves. Finally, 3.0 g of solid SSZ13 were added into 0.1 M NaOH aqueous solution, stirring for 2 h at 80 °C. The above etched SSZ13 were centrifuged and washed with deionized water for three times. The resulting sample was dried at 80 °C for 12 h, which was denoted as hollow SSZ13.

Preparation of hollow Zn-SSZ13 molecular sieve

1.0 g of hollow SSZ13 samples were dispersed in 80 mL of 1 M NH_4Cl solution with a magnetic stirring at 80 °C for 6 h. The resultant precipitate was washed with deionized H_2O for five times. After dried at 80 °C for 3 h, the obtained sample was denoted as NH_4-SSZ13. Then, 1.0 g of NH_4-SSZ13 powders were added into 80 mL of 0.1 M $ZnCl_2$ solution, which was stirred at 80 °C for additional 6 h. After the subsequent washing and drying treatments, the acquired powders were ultimately calcinated in a muffle oven at 500 °C for 6 h with a heating rate of 5 °C min^{-1}, labeled as hollow Zn-SSZ13 for further use (abbreviated as Z).

Preparation of artificial SEI on the Zn/Cu foil

X g of hollow Zn-SSZ13 (Z) and Y g of carrageenan (abbreviated as C) were uniformly dispersed in 20 mL of deionized H_2O, which was marked as ZC-X-Y (X:Y = 9:1, 8:2, and 7:3, respectively). Then, the gel was bladed onto the Zn/Cu foil with a thickness of W μm (W = 50, 100, 200 μm, respectively). After air-dried at room temperature, the Zn/Cu foil was cut into discs with a diameter of 10 mm. The obtained Zn and Cu electrodes were labeled as ZC-X-Y-W@Zn and ZC-X-Y-W@Cu, respectively. The artificial SEI of pure carrageenan and hollow Zn-SSZ13

were also coated on the Zn/Cu foils, which were marked as C-W@Zn/C-W@Cu and Z-W@Zn/Z-W@Cu, respectively.

Preparation of α-MnO_2 electrode

The α-MnO_2 materials were synthesized according to a reported work.[S2] 0.37 g of $MnSO_4 \cdot H_2O$ was evenly dispersed in 20 mL of deionized water, and 0.23 g of $KMnO_4$ was added into 20 mL of deionized water. Then, both the above solutions were uniformly mixed by stirring for 3 h. The obtained solution was transferred into a Teflon-lined autoclave, which was subjected to a hydrothermal reaction at 160 °C in an oven for 12 h. The generated sediments were centrifuged and rinsed with deionized water for five times, and the cleaned samples were evaporated at 80 °C in a vacuum oven for 12 h. Subsequently, the MnO_2, polyvinylidene difluoride (PVDF), and carbon black (CB) materials with a weight ratio of 7:1:2 were uniformly dispersed into the N-methyl-2-pyrrolidone (NMP) solvents. The prepared slurry was scraped on a stainless steel (SS) foil, which was placed in a vacuum oven at 80 °C for 12 h. The loading mass of active material was approximately 0.7 mg cm^{-2}. Ultimately, the SS electrodes coated with MnO_2 materials were cut into discs with a diameter of 10 mm, which were utilized as the cathodes in Zn||MnO_2 full batteries.

Preparation of $Na_2V_6O_{16} \cdot 1.5H_2O$ electrode

The $Na_2V_6O_{16} \cdot 1.5H_2O$ (NVO) nanorods were synthesized on the basis of the previous approach.[S3] 1.80 g of V_2O_5 and 0.40 g of NaOH were simultaneously dissolved by 40 mL of deionized water. The even solution was added into a teflon-lined stainless-steel autoclave, which was kept at 180 °C for 40 h. The products were washed with deionized water for six times. The final NVO products can be acquired through the freeze-drying process. To prepare the NVO electrodes, the NVO, CB, and PVDF with a weight ratio of 7:2:1 were evenly dispersed into the NMP solvents. The mixed slurry was coated on a SS foil and subsequently placed in a vacuum oven at 80 °C for 12 h. The loading mass of active material was around 2.1 mg cm^{-2}. Ultimately, the NVO electrodes were tailored into 6 cm^2 (2 cm × 3 cm) slices, which were employed as the cathodes in Zn||NVO pouch cells.

Material characterization

The chemical and structural functional groups were determined via fourier transform infrared (FTIR, Nicolet 8700). The morphology and structure were observed by high resolution transmission electron microscopy (TEM, JEM-2100 Plus) and field emission scanning electron microscopy (SEM, GeminiSEM 450). The distribution of the various elements (Zn, O, Si, and Al)

on Zn-SSZ13 were characterized using SEM equipped with an energy-dispersive X-ray (EDX) spectroscopy. The Raman spectra were obtained via Confocal Raman System (Horiba LabRAM SoLeil, 532 nm wavelength). X-ray photoelectron spectroscopy (XPS, ESCALab220i-XL) without the treatment of Ar^+ sputtering depth was employed for the analysis of surface chemical valence states. Crystal texture on the metallic foil surface was determined by X-ray diffraction (XRD, SmartLab) with Cu Kα radiation (λ = 1.54 Å). Crystal texture analysis was conducted on High-Resolution X-ray Diffractometer (XPert3 MRD) at 12 kV and 40 mA (Cu Kα radiation, λ = 1.5406 Å). 2D wide-angle X-ray scattering (WAXS) measurements were performed at 30 W with Cu Kα radiation (λ = 1.54189 Å). The evolution of the Zn dendrite growth at the electrode interface was monitored via in-situ optical microscope (YueScope, YM710TR).

Electrochemical measurements

The cyclic voltammetry (CV), chronoamperometry (CA), electrochemical impedance spectroscopy (EIS), Tafel plot, and linear sweep voltammetry (LSV) were performed via the CHI760E electrochemical workstation. CV curves of the Zn||MnO_2 full cells were carried out at a scanning rate of 1 mV s^{-1} from 0.8 to 1.8 V. CA profiles were obtained at a fixed overpotential of −150 mV. EIS plots were measured at a frequency from 0.01 Hz to 100 kHz with an amplitude of 10 mV. Tafel patterns were obtained at a sweeping speed of 5 mV s^{-1} from –1.2 to –0.8 V, where a three-electrode system was used including the Zn foil as the work electrode, the Ag/AgCl as the reference electrode, and the graphite rod as the counter electrode. Hydrogen evolution reaction (HER) curves were performed according to the LSV measurement between –1.6 V and –1.1 V at a scan rate of 5 mV s^{-1}.

The Zn||Zn symmetrical cells, Zn||Cu half cells, and Zn||MnO_2 full cells were assembled utilizing CR2032 coin-type cells, which were further evaluated on a LAND battery system. The thickness of the commercial Zn foil was about 50 μm. 100 μL of $ZnSO_4$ aqueous solution (2 M) was employed as the electrolytes for symmetrical cells and half cells, and 100 μL of the mixed electrolytes (2 M $ZnSO_4$ and 0.1 M $MnSO_4$) was adopted in the Zn||MnO_2 full cells. The addition of extra Mn^{2+} ions could promote the structure stability of the MnO_2 electrode through the inhibition of disproportionation reactions. The plating experiments were performed at a current density of 2 mA cm^{-2} with an areal capacity of 10 mAh cm^{-2}. The rate capability of the Zn||Zn symmetrical cells were evaluated at various current densities of 1.0, 5.0, 10.0, and 25.0 mA cm^{-2} with a fixed areal capacity of 1 mAh cm^{-2}. Galvanostatic charge/discharge (GCD) measurements of the Zn||MnO_2 full cells were carried out using the LAND battery system with no resting time.

The rate capability of the Zn||MnO_2 full cells were carried out at different current densities of 0.2, 0.5, 1.0, 2.0, 5.0, 10.0, and 20.0 A g^{-1}. The long-term cycling performance of the Zn||MnO_2 full cells was measured at 0.2 A g^{-1} for activation (10 cycles) without standing time, followed by long-term testing at 1.0 A g^{-1}. 1.0 mL of composite electrolyte (2 M $ZnSO_4$ and 1 M Na_2SO_4) was utilized for the Zn||NVO pouch cells, and the additional Na^+ ions could enhance the structural stability of the NVO electrode. The assembled Zn||NVO pouch cells were assessed at 0.5 A g^{-1} in a LAND battery system.

Density functional theory (DFT) computations

DFT calculations were performed in terms of the Vienna Ab-inito Simulation Package (VASP).[S4,S5] The Perdew-Burke-Ernzerhof (PBE) functional within the generalized gradient approximation (GGA) methodology was utilized to describe the exchange-correlation effects.[S6.S7] Meanwhile, the core-valence interactions were ascribed to the projected augmented wave (PAW) approach.[S8] Subsequently, the energy cutoff for plane wave expansions was set to 400 eV, and the structural optimization was completed with energy and force convergence criteria set at 1.0×10^{-4} eV and 0.05 eV $Å^{-1}$, respectively. Furthermore, the Brillouin zone was sampled with the 1×1×1 K-point. Finally, the Grimme's DFT-D3 methodology was employed to describe the dispersion interactions.[S9]

The adsorption energy (E_{ads}) of the —OSO_3^- and —OH groups in the κ-carrageenan molecules were computed by following equation:

$$E_{ads} = E_{*\kappa-carrageenan} - E_{\kappa-carrageenan} - E_{sub} \quad (1)$$

where $E_{\kappa\text{-carrageenan}}$ and $E_{*\kappa\text{-carrageenan}}$ correspond to the energies before and after the adsorption of the groups (—OSO_3^- and —OH) in the κ-carrageenan molecules on the substrates, respectively. E_{sub} represents the energy of the constructed Zn-002, Zn-100 and Zn-101 substrates.

Electric field simulations

The simplified 2D model served for the calculation of the interfacial electric field distribution in terms of COMSOL Multiphysics. The ionic conductivity in the $ZnSO_4$ solution (2.0 M) was around 3.0 S m^{-1} by a previous report.[S10] The local current density was computed via the Butler-Volmer equation (**Equation** 2):[S11-S13]

$$i = i_0(C_R e^{\frac{\alpha_a \eta F}{RT}} - C_O e^{\frac{-\alpha_c \eta F}{RT}}) \quad (2)$$

where i is charge transfer current density, i_0 refers to exchange current density, C_R and C_O correspond to the concentrations of reduction and oxidation species, α_a and α_c are attributed to the coefficients of anodic and cathodic charge transfer, η represents activation overpotential, F is Faraday constant, R is assigned to ideal gas constant, T refers to Kelvin temperature. Nevertheless, this designed model merely exhibits an idealized system that falls short of fully capturing the inherent intricacies in real-world conditions.

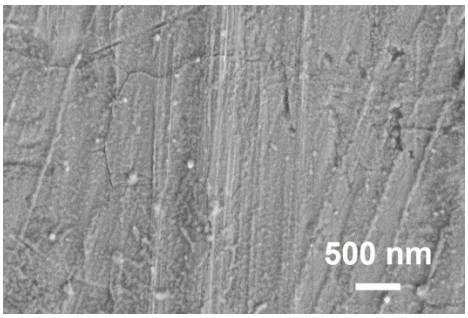

Fig. S1 Magnified SEM image of the bare Zn.

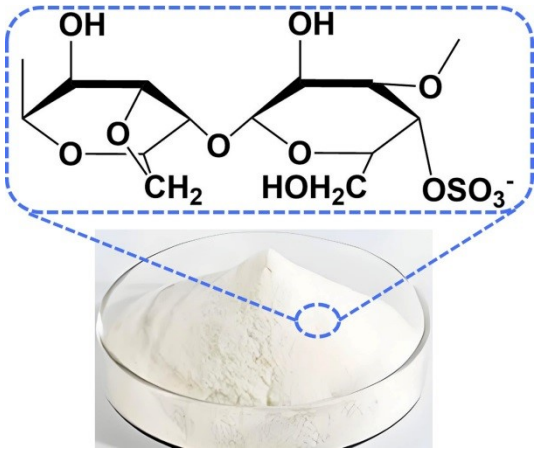

Fig. S2 The utilized carrageenan powders and the microscopic structure of the monomer molecule.

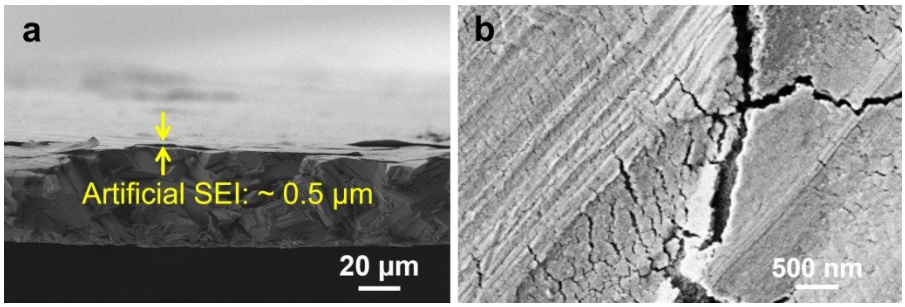

Fig. S3 (a) Cross-section SEM image of C-50@Zn. (b) Enlarged SEM image of C-50@Zn.

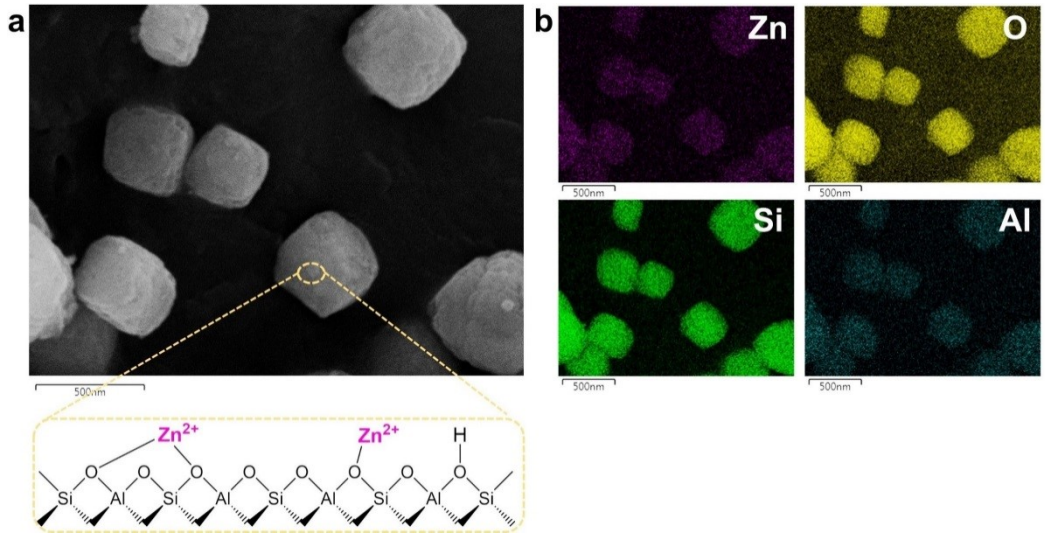

Fig. S4 (a) Top-view SEM image of the Zn-SSZ13 molecular sieves with its possible micro-configuration. (b) Corresponding EDS mapping of the prepared Zn-SSZ13 materials.

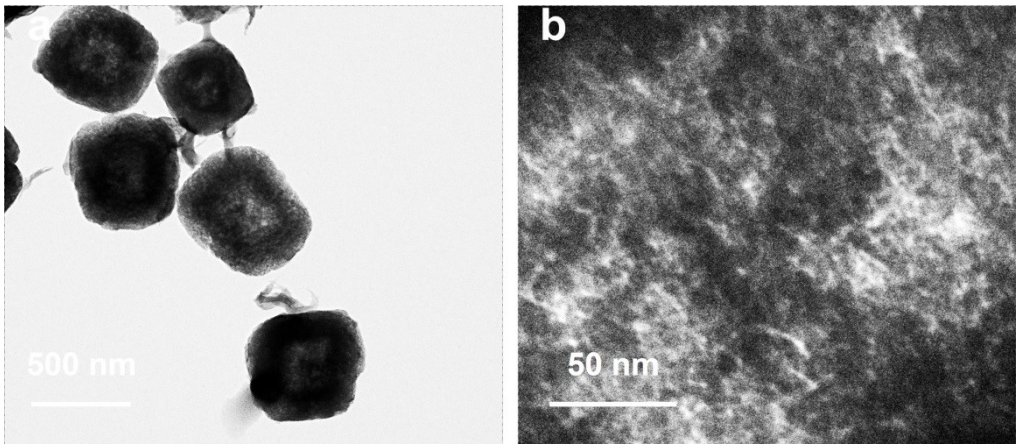

Fig. S5 (a) HRTEM image of the hollow Zn-SSZ13 nanoparticles. (b) Corresponding enlarged image of the hollow Zn-SSZ13.

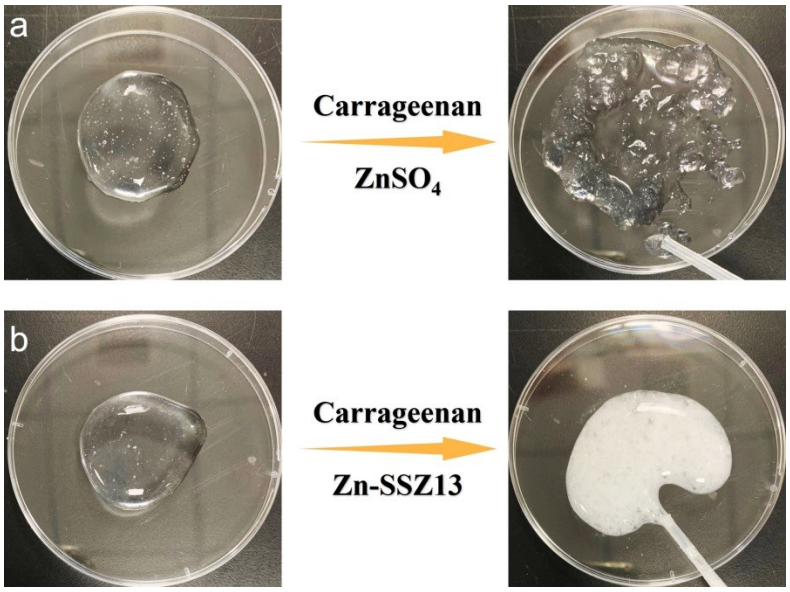

Fig. S6 Photographs of the carrageenan aqueous solution before and after the addition of (a) $ZnSO_4$ and (b) Zn-SSZ13.

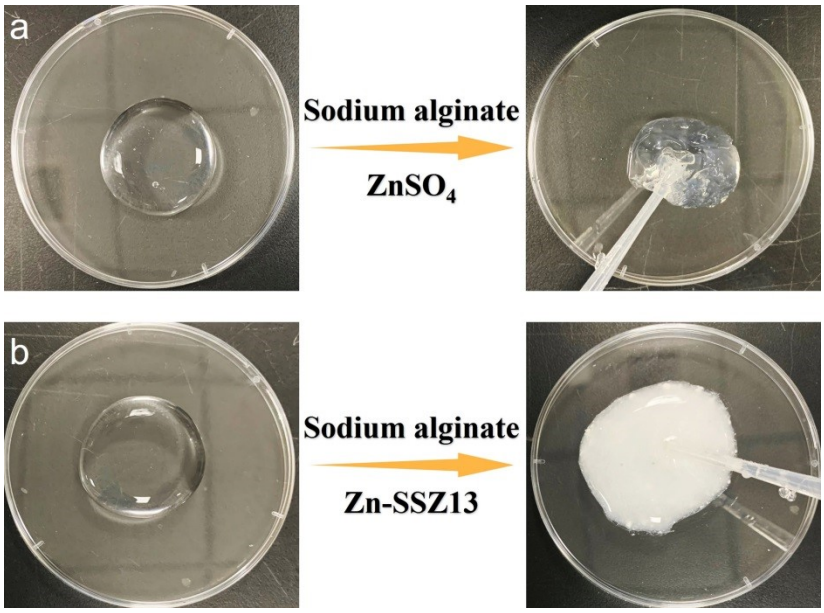

Fig. S7 Photographs of the sodium alginate aqueous solution before and after the addition of (a) $ZnSO_4$ and (b) Zn-SSZ13.

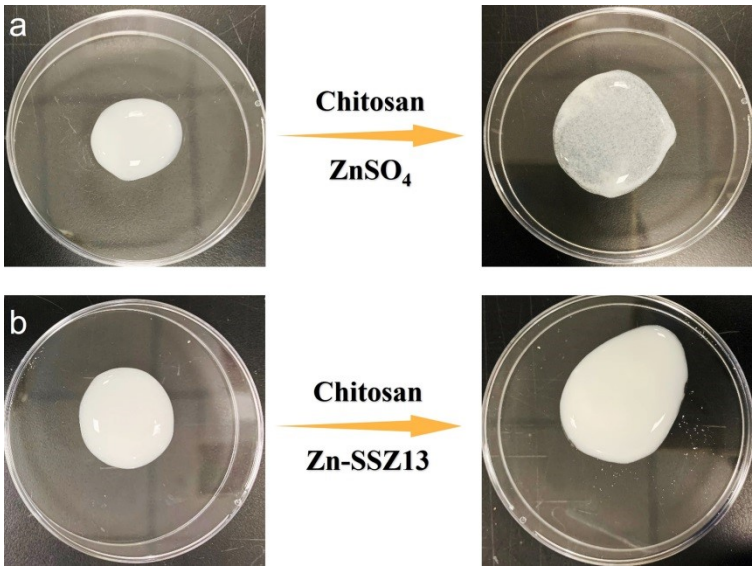

Fig. S8 Photographs of the chitosan aqueous solution before and after the addition of (a) $ZnSO_4$ and (b) Zn-SSZ13.

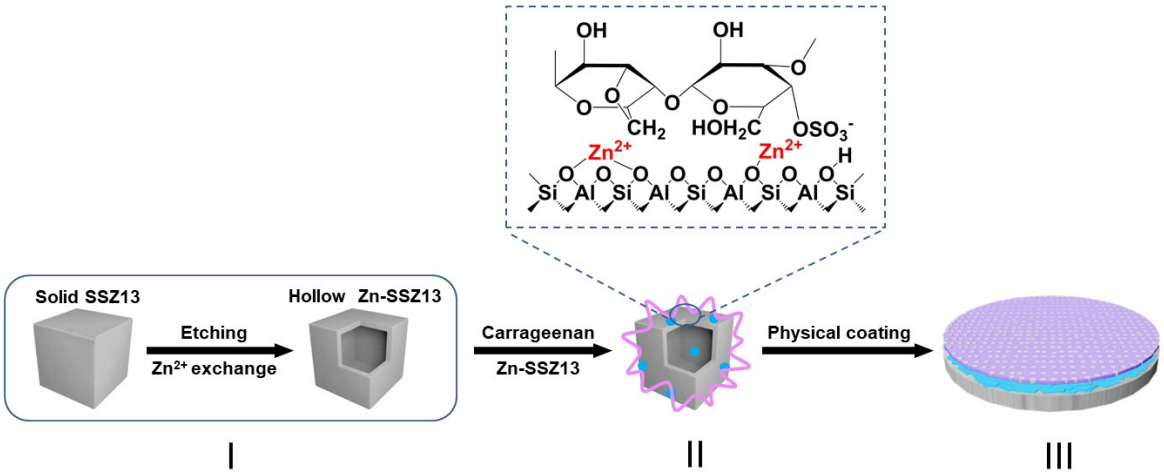

Fig. S9 Schematic illustration for the preparation of the hollow Zn-SSZ13 and the ZC-8-2-50@Zn electrode.

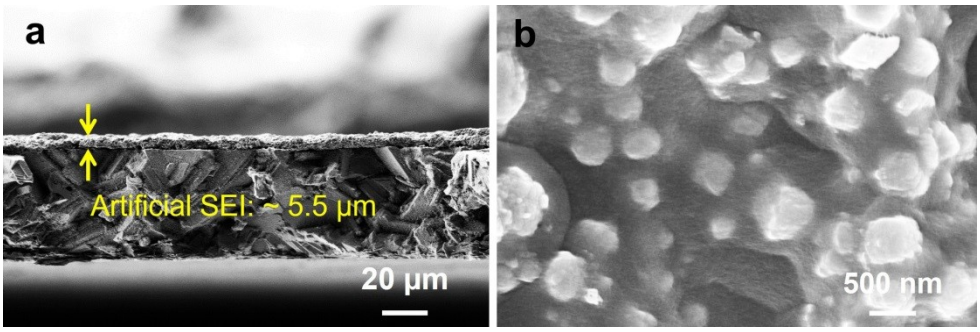

Fig. S10 (a) Cross-section SEM image of ZC-8-2-50@Zn. (b) Magnified SEM image of ZC-8-2-50@Zn.

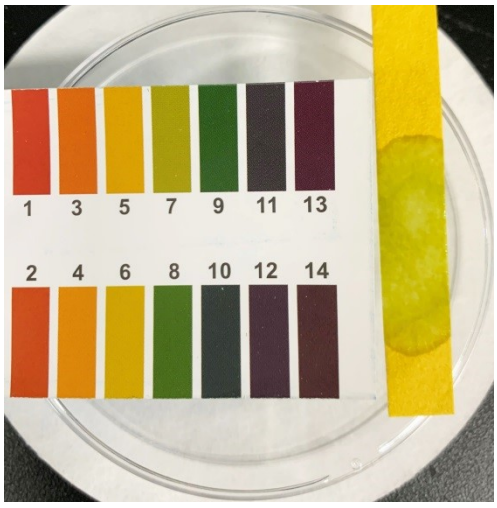

Fig. S11 Optical photo for the pH of the pure carrageenan solution.

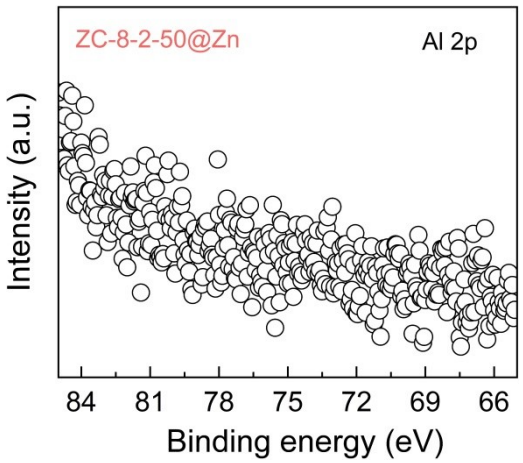

Fig. S12 Al2p spectra for the ZC-8-2-50@Zn with surface coatings removed.

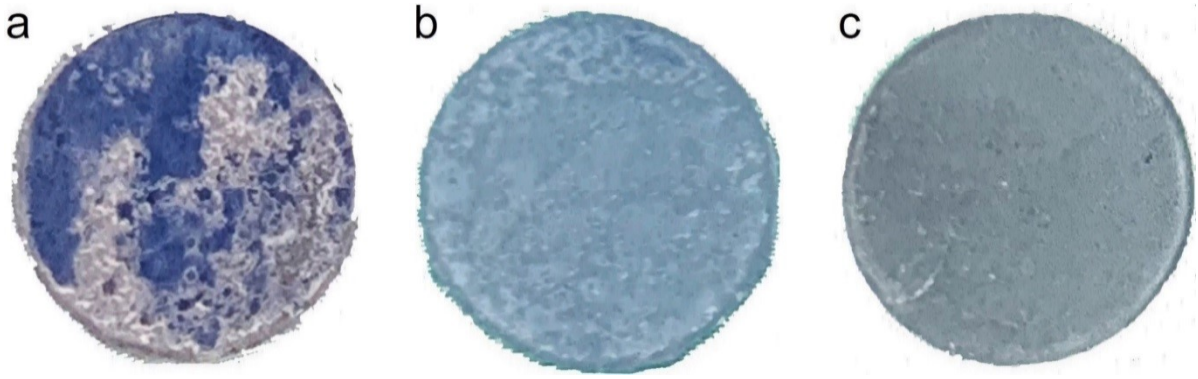

Fig. S13 Optical pictures of the plated (a) bare Zn, (b) C-50@Zn, and (c) ZC-8-2-50@Zn electrodes at 2 mA cm^{-2} and 10 mAh cm^{-2}.

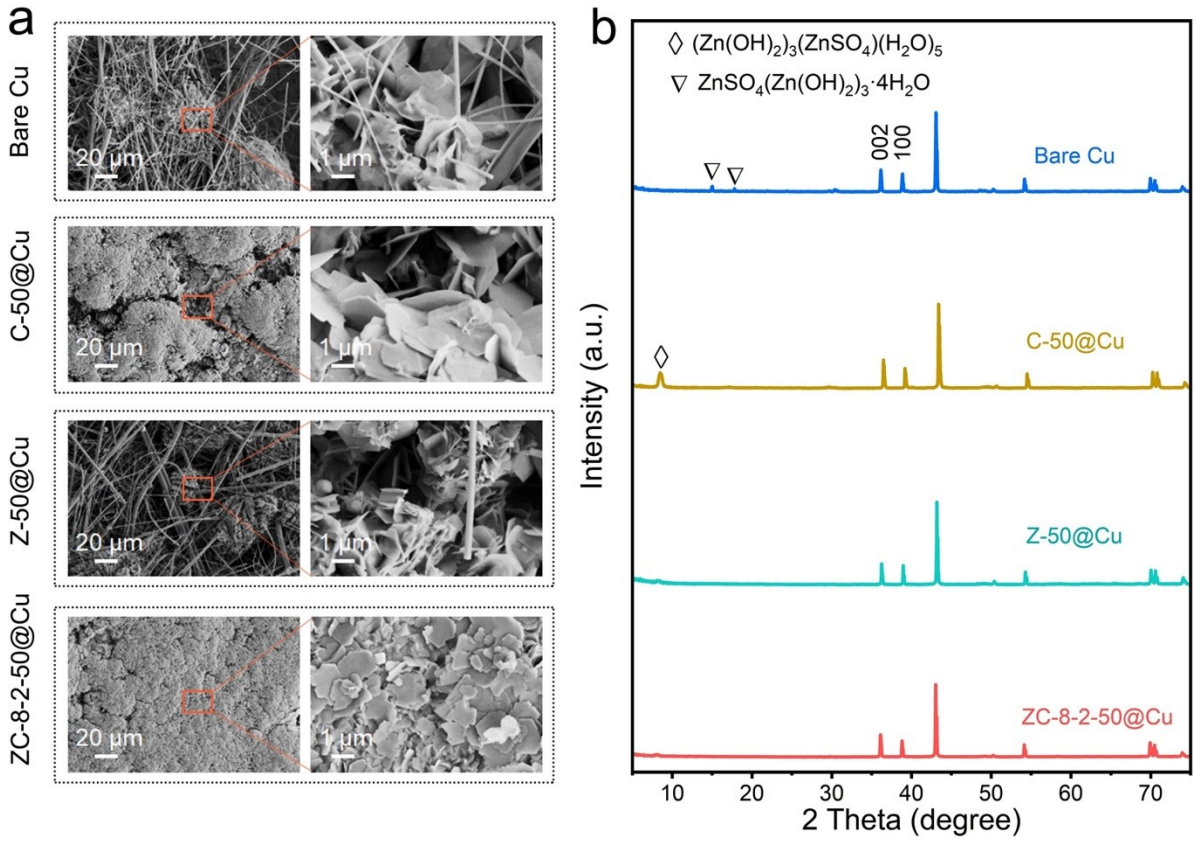

Fig. S14 (a) Top-view SEM images of plated bare Cu, C-50@Cu, Z-50@Cu, and ZC-8-2-50@Cu electrodes after Zn deposition at 2 mA cm^{-2} and 10 mAh cm^{-2}. (b) Corresponding XRD patterns of plated bare Cu, C-50@Cu, Z-50@Cu, and ZC-8-2-50@Cu electrodes.

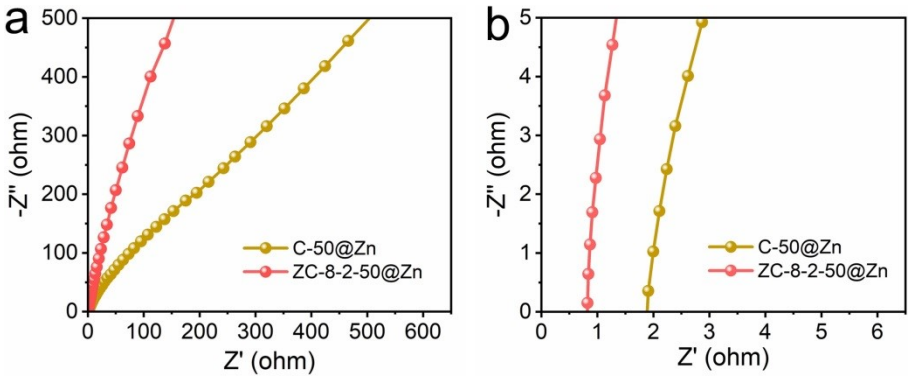

Fig. S15 (a) Nyquist plots of Zn anodes with different protective layers. (b) Enlarged spectra of the high frequency region in (a).

Supporting notes:

The ionic conductivity (σ) is estimated on the basis of the following equation:[S14,S15]

$$\sigma = \frac{l}{R_b S}$$

where R_b represents the bulk resistance based on the EIS measurement (R_b(C-50) = 1.87 ohm and R_b(ZC-8-2-50) = 0.83 ohm), l refers to the thickness of the C-50 (0.00015 cm) and ZC-8-2-50 coating layers (0.001 cm), and S is the contact area between the electrode and electrolyte (0.785 cm^{-2}). Therefore, the ionic conductivity of the C-50 and ZC-8-2-50 were 1.55 mS cm^{-1} and 0.11 mS cm^{-1}, respectively.

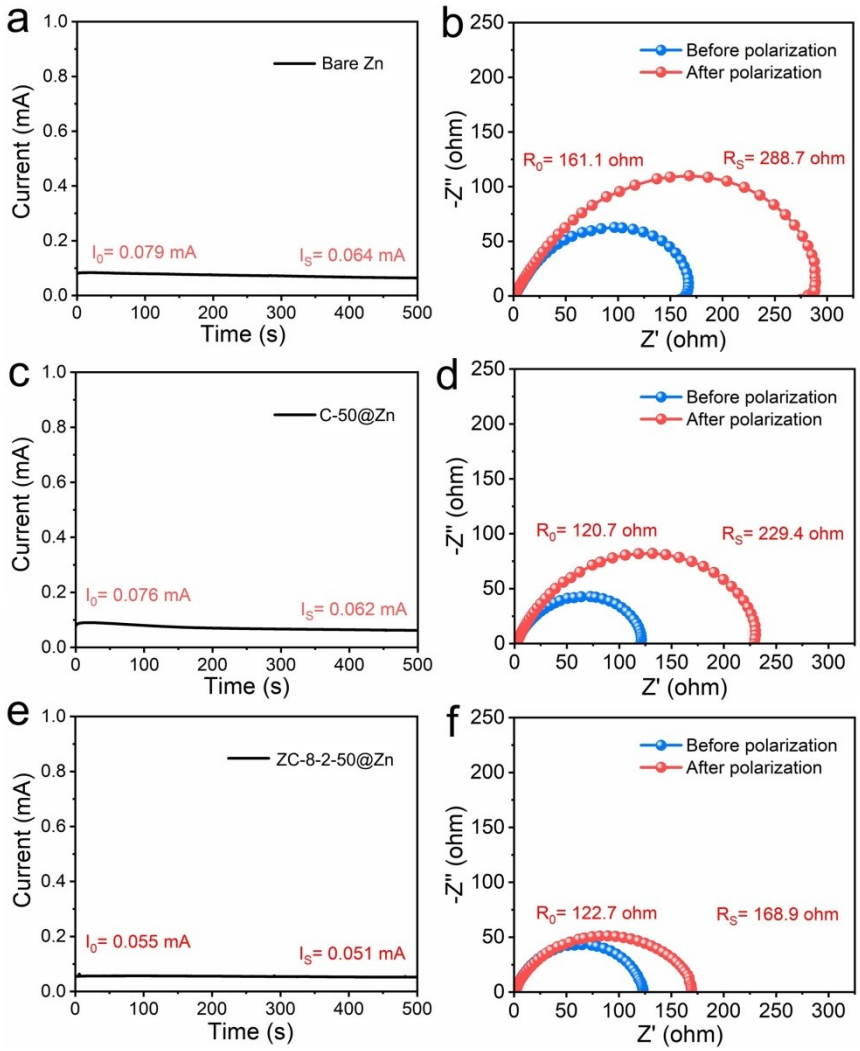

Fig. S16 Current-time plots and EIS spectra before and after polarization of the symmetrical batteries assembled by various electrodes of (a-b) bare Zn, (c-d) C-50@Zn, and (e-f) ZC-8-2-50@Zn.

Supporting notes:

The Zn^{2+} transference number (t_+) is estimated utilizing the typical Bruce-Vincent method via the following equation:[S16]

$$t_+ = \frac{I_s(\Delta V - I_0 R_0)}{I_0(\Delta V - I_s R_s)}$$

where ΔV is the constant polarization voltage (10 mV), I_0 (0.079 mA for bare Zn, 0.076 mA for C-50@Zn, and 0.055 mA for ZC-8-2-50@Zn) and R_0 (~161.1 ohm for bare Zn, ~120.7 ohm for C-50@Zn, and ~122.7 ohm for ZC-8-2-50@Zn) are the initial current and charge transfer resistance, I_s (0.064 mA for bare Zn, 0.062 mA for C-50@Zn, and 0.051 mA for ZC-8-2-50@Zn) and R_s (~288.7 ohm for bare Zn, ~229.4 ohm for C-50@Zn, and ~168.9 ohm for ZC-8-2-50@Zn) are the steady-state current and charge transfer resistance, respectively.

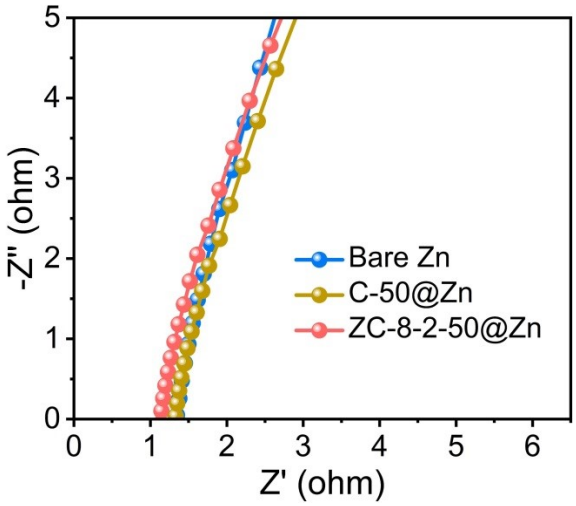

Fig. S17 Magnified high frequency Nyquist plots of the symmetrical cells assembled by the bare Zn, C-50@Zn, and ZC-8-2-50@Zn electrodes in **Fig. 3c**.

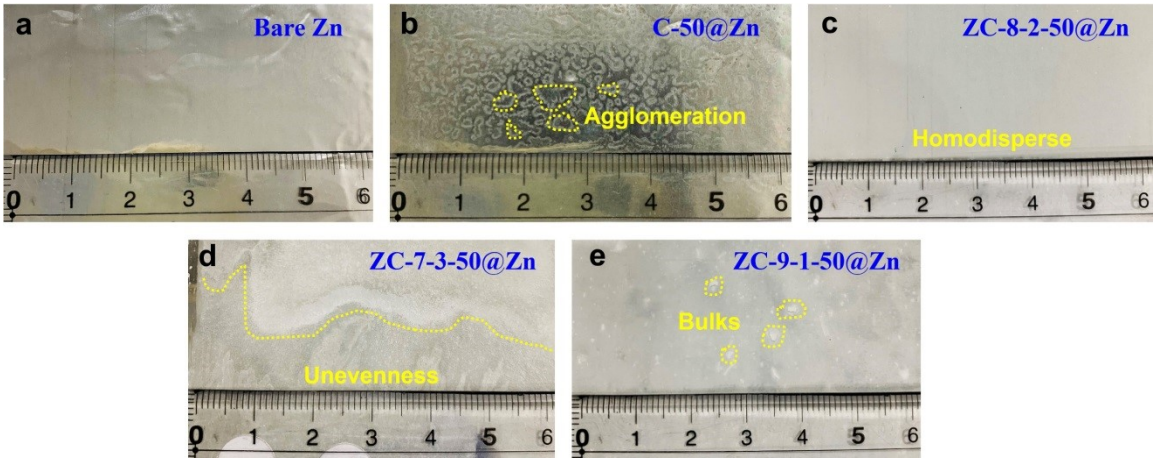

Fig. S18 Optical pictures of the surface morphology on the different electrodes. (a) bare Zn, (b) C-50@Zn, (c) ZC-8-2-50@Zn, (d) ZC-7-3-50@Zn, and (e) ZC-9-1-50@Zn.

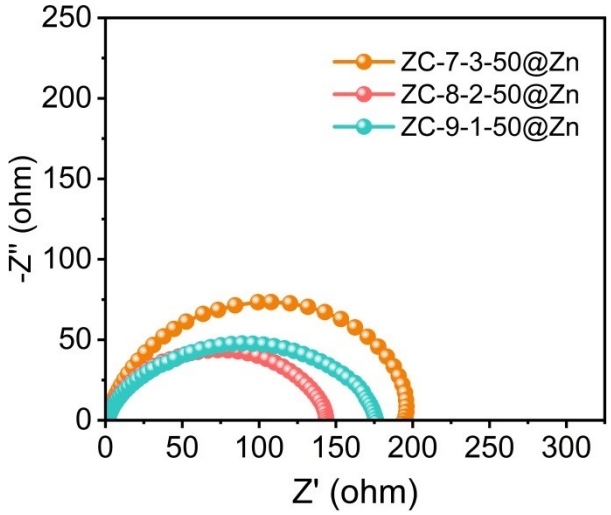

Fig. S19 EIS plots of the symmetrical cells assembled by the ZC-7-3-50@Zn, ZC-8-2-50@Zn, and ZC-9-1-50@Zn electrodes.

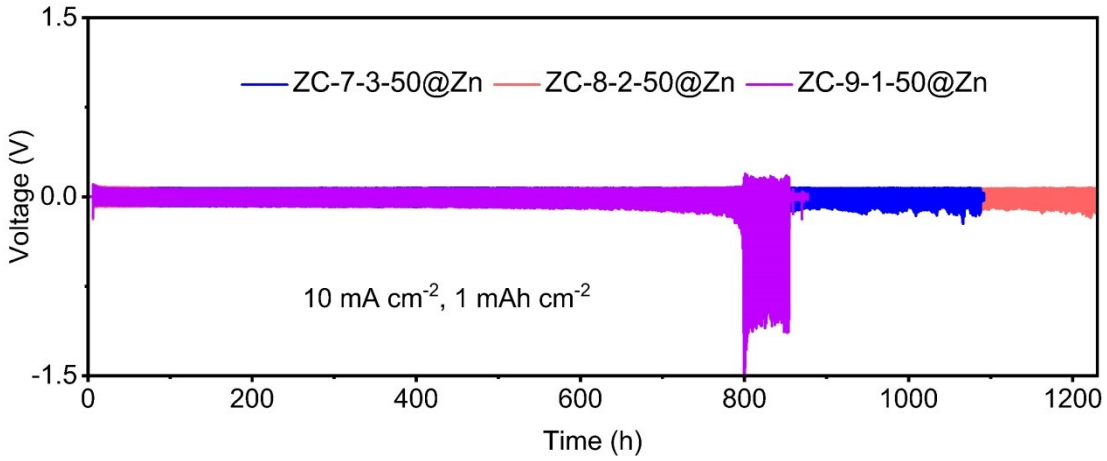

Fig. S20 Voltage profiles of the symmetrical batteries assembled by the ZC-7-3-50@Zn, ZC-8-2-50@Zn, and ZC-9-1-50@Zn electrodes at 10 mA cm^{-2} and 1 mAh cm^{-2}.

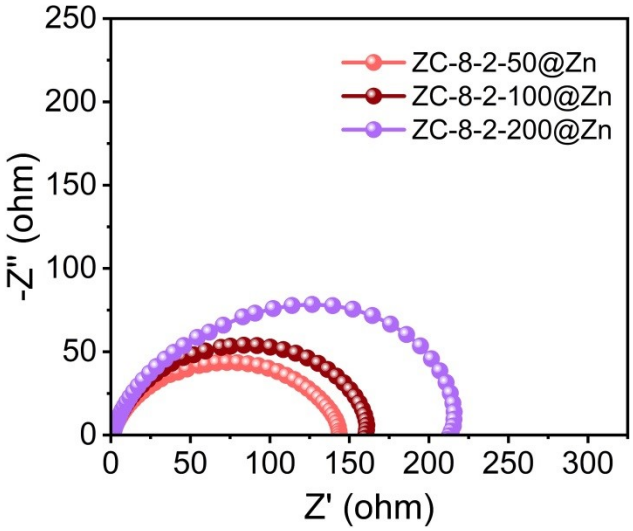

Fig. S21 EIS plots of the symmetrical cells assembled by the ZC-8-2-50@Zn, ZC-8-2-100@Zn, and ZC-8-2-200@Zn electrodes.

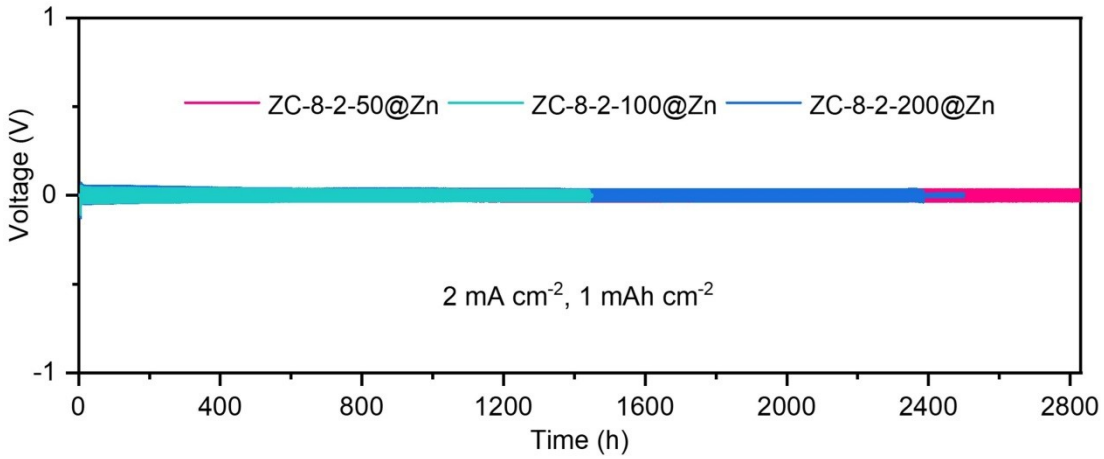

Fig. S22 Voltage profiles of the symmetrical cells assembled by the ZC-8-2-50@Zn, ZC-8-2-100@Zn, and ZC-8-2-200@Zn electrodes at 2 mA cm^{-2} and 1 mAh cm^{-2}.

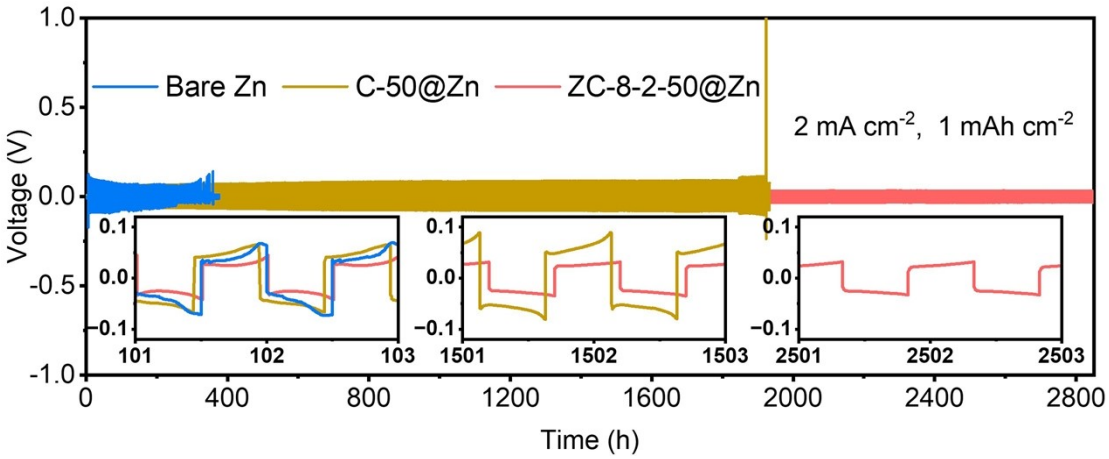

Fig. S23 Galvanostatic cycling performance of the ZC-8-2-50@Zn||ZC-8-2-50@Zn symmetrical cell at 2 mA cm^{-2}, 1 mAh cm^{-2}.

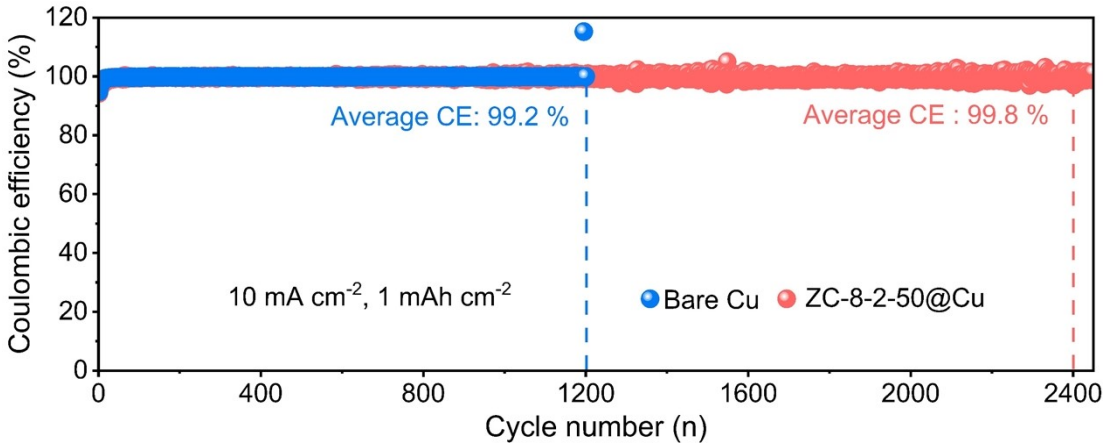

Fig. S24 Average Zn^{2+} plating/stripping CEs of bare Zn||bare Cu and bare Zn||ZC-8-2-50@Cu asymmetrical cells at 10 mA cm^{-2} and 1 mAh cm^{-2}.

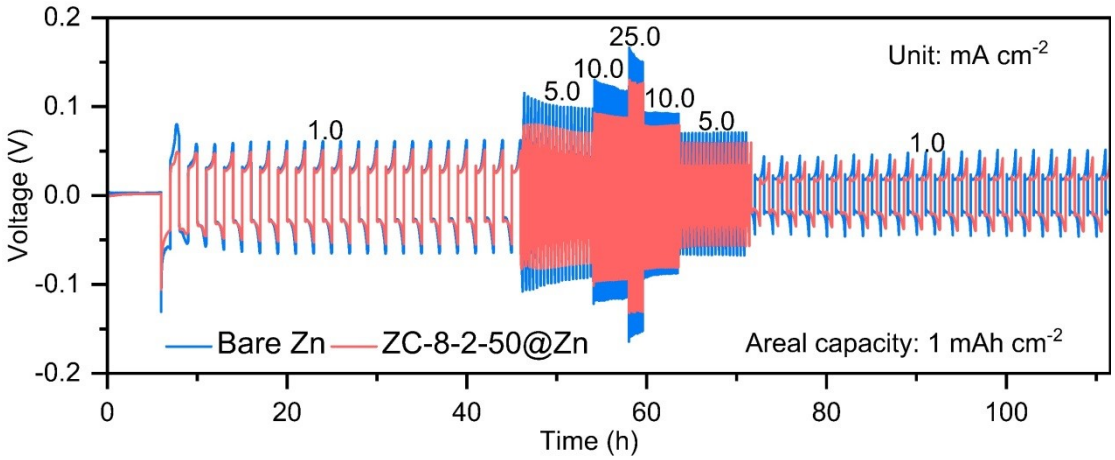

Fig. S25 Rate performance of bare Zn||bare Zn and ZC-8-2-50@Zn||ZC-8-2-50@Zn symmetrical cells at various current densities with a constant capacity of 1 mAh cm^{-2}.

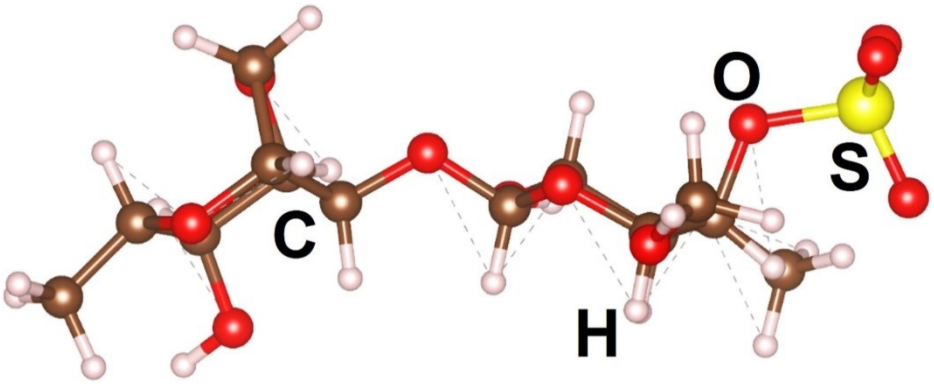

Fig. S26 Constructed adsorption molecule of the carrageenan monomer.

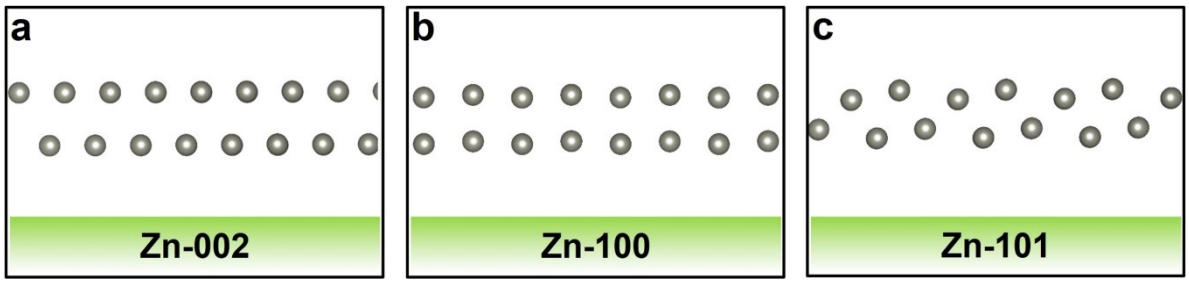

Fig. S27 Constructed adsorption substrates of (a) Zn-002, (b) Zn-100, and (c) Zn-101 lattice planes.

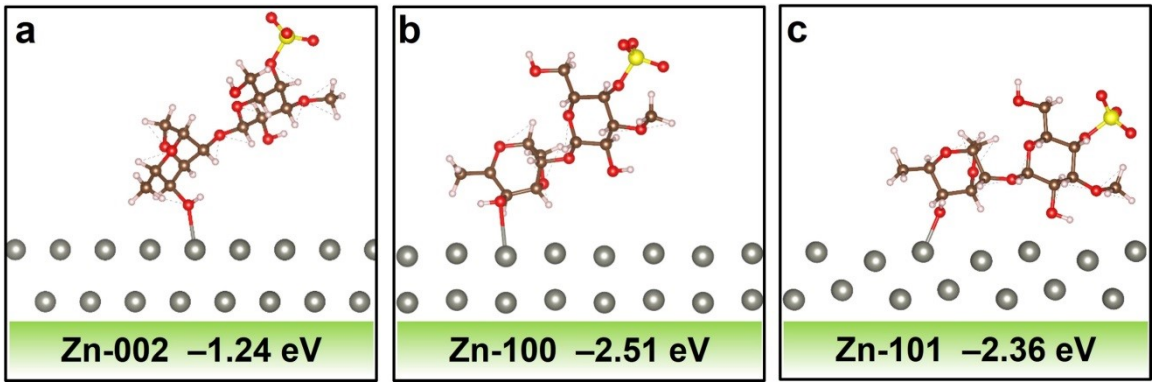

Fig. S28 Calculated adsorption energies of the —OH groups in the carrageenan monomers on diverse Zn facets of (a) Zn-002, (b) Zn-100, and (c) Zn-101.

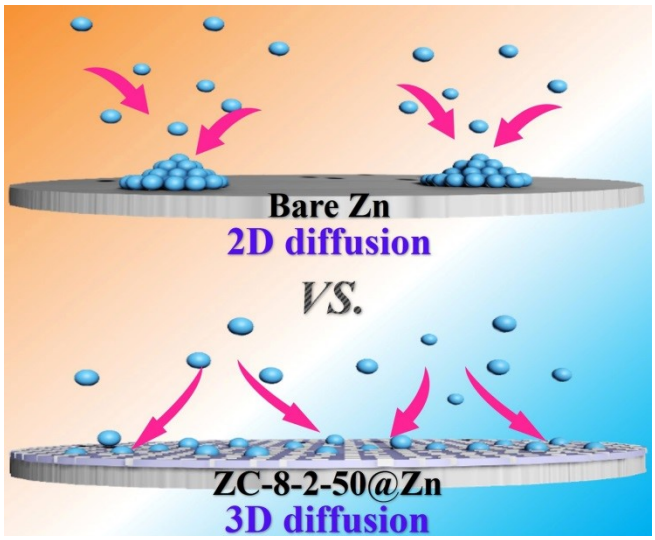

Fig. S29 Schematic diagram for the diffusion and deposition processes of interfacial Zn^{2+} ions on both bare Zn and ZC-8-2-50@Zn electrodes.

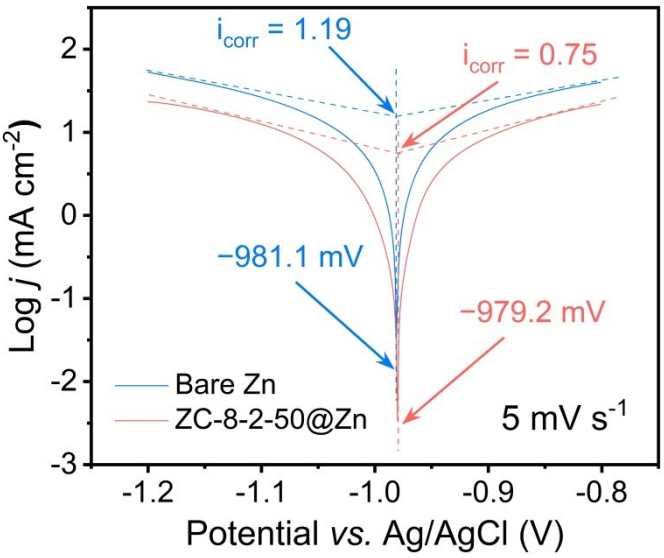

Fig. S30 Tafel plots of the bare Zn and ZC-8-2-50@Zn electrodes at a scan rate of 5 mV s^{-1}.

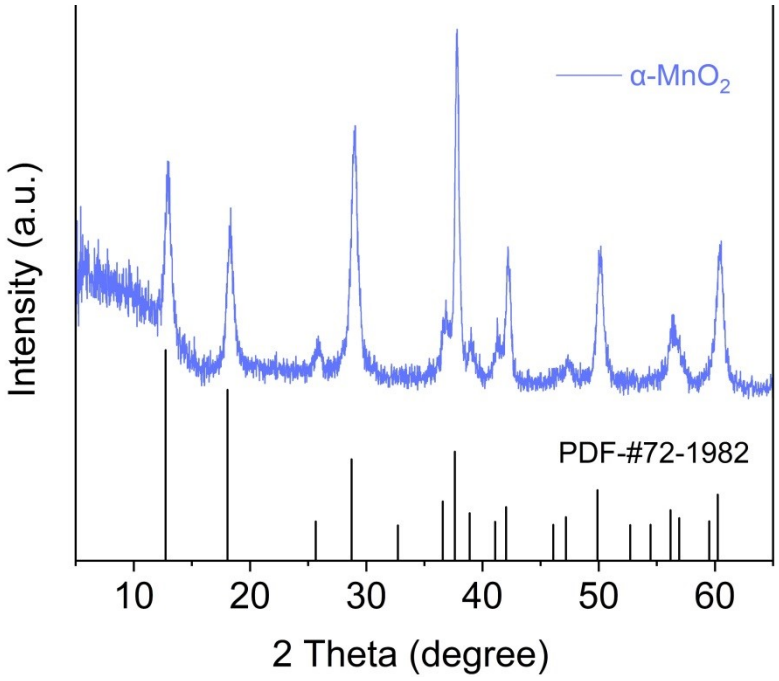

Fig. S31 XRD patterns of the prepared α-MnO_2 materials.

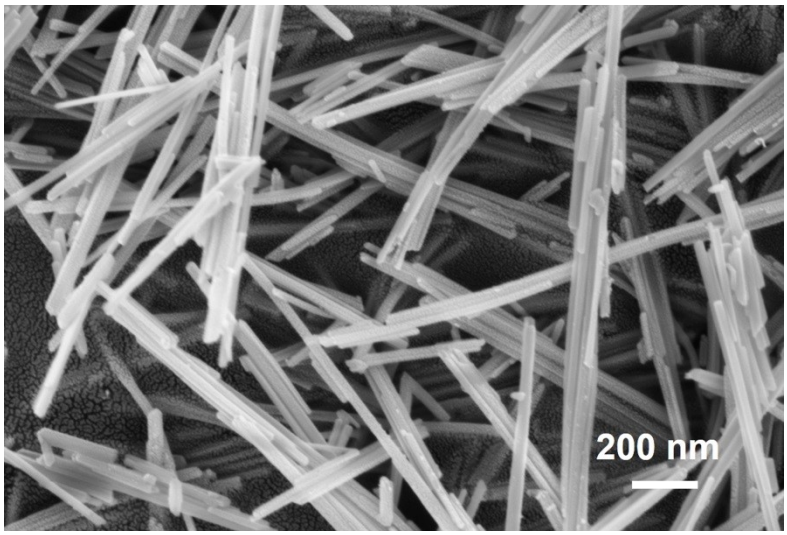

Fig. S32 SEM image of the prepared α-MnO_2 materials.

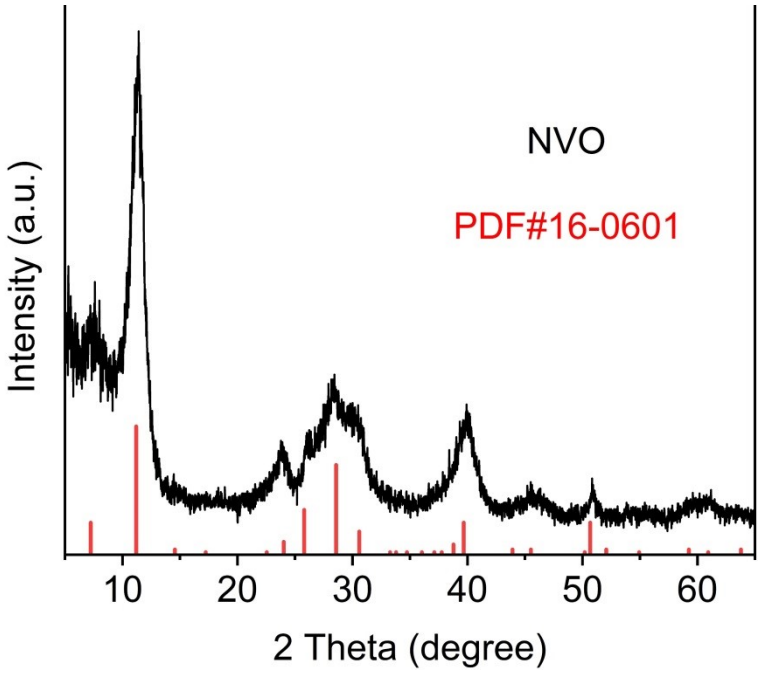

Fig. S33 XRD patterns of the synthesized NVO materials.

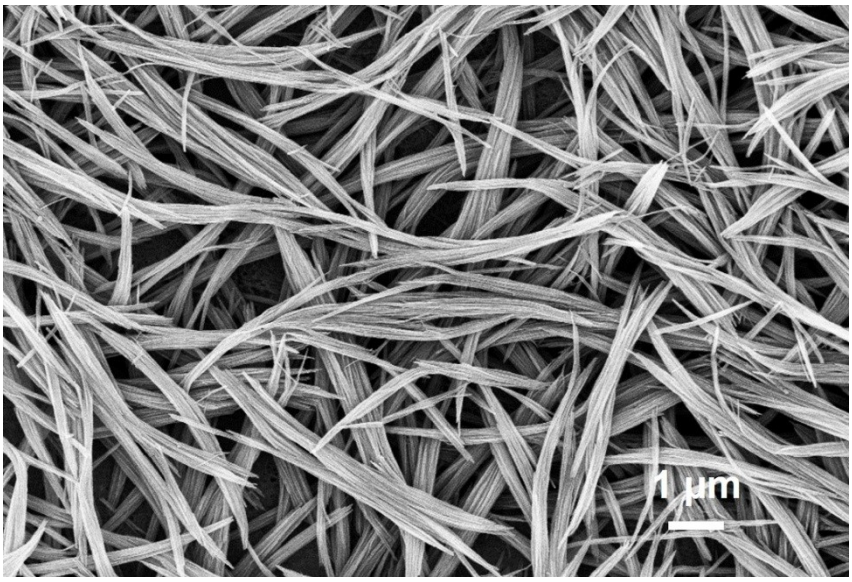

Fig. S34 SEM image of the synthesized NVO materials.

Fig. S35 Optical picture of the ZC-8-2-50@Zn||NVO pouch cell before bent and pierced examinations.

Table S1 Galvanostatic plating/stripping performance of this work and the recently reported Zn||Zn symmetrical cells.

Anode	Current density / mA cm^{-2}	Areal capacity / mAh cm^{-2}	Voltage hysteresis at 100 h / mV	Life time / h	Cumulative plating capacity/ mAh cm^{-2}	Depth of discharge/ %	Ref.
ZnSe@Zn	30.0	10.0	145	170	2549	17.1 %	S17
With DA	10.0	10.0	97	200	1000	28.5 %	S18
(002)-Zn	10.0	10.0	100	210	1050	30.3 %	S19
Zn@ZBO	50.0	10.0	240	250	6250	57.0 %	S20
ZG@Zn	20.0	10.0	150	105	1050	6.8 %	S21
DCP-Zn-30	5.0	10.0	90	200	500	14.3 %	S22
Sac/$ZnSO_4$	40.0	10.0	250	220	4400	24.4 %	S23
Zn@NH_2-$PSiO_x$	20.0	10.0	130	300	3000	57.0 %	S24
Zn@ZnF_2	10.0	10.0	70	600	3000	8.6 %	S25
Zn/INS	20.0	20.0	30	80	800	13.7 %	S26
ZnSe@Zn	30.0	10.0	91	172	2579	17.1 %	S27
USL-Zn	15.0	15.0	150	100	750	51.3 %	S28
ZC-8-2-50@Zn	25.0	10.0	94	830	10375	34.2 %	This work

References

S1 X. Zhang, Z. Wang, Z. Chen, Y. Zhu, Z. Liu, F. Li, W. Zhou, Z. Dong, J. Fan and L. Liu, *Appl. Catal. B-Environ.*, 2022, **317**, 121771.

S2 C. Deng, X. Xie, J. Han, B. Lu, S. Liang and J. Zhou, *Adv. Funct. Mater.*, 2021, **31**, 2103227.

S3 F. Wan, L. Zhang, X. Dai, X. Wang, Z. Niu and J. Chen, *Nat. Commun.*, 2018, **9**, 1656.

S4 G. Kresse and J. Hafner, *Phys. Rev. B*, 1993, **47**, 558.

S5 G. Kresse and J. Hafner, *Phys. Rev. B*, 1994, **49**, 14251.

S6 J. Perdew, K. Burke and M. Ernzerhof, *Phys. Rev. Lett.*, 1996, **77**, 3865.

S7 G. Kresse and D. Joubert, *Phys. Rev. B*, 1999, **59**, 1758.

S8 P. Blochl, *Phys. Rev. B*, 1994, **50**, 17953.

S9 S. Grimme, J. Antony, S. Ehrlich and H. Krieg, *J. Chem. Phys.*, 2010, **132**, 154104.

S10 Q. Cao, Y. Gao, J. Pu, X. Zhao, Y. Wang, J. Chen and C. Guan, *Nat. Commun.*, 2023, **14**, 641.

S11 W. Wang, G. Huang, Y. Wang, Z. Cao, L. Cavallo, M. Hedhili and H. Alshareef, *Adv. Energy Mater.*, 2022, **12**, 2102797.

S12 Z. Guo, L. Fan, C. Zhao, A. Chen, N. Liu, Y. Zhang and N. Zhang, *Adv. Mater.*, 2022, **34**, 2105133.

S13 Z. Wang, Y. Huang, K. Xu, Y. Zhong, C. He, L. Jiang, J. Sun, Z. Rao, J. Zhu, J. Huang, F. Xiao, H. Liu and B. Xia, *Nat. Commun.*, 2023, **14**, 69.

S14 K. Zhao, G. Fan, J. Liu, F. Liu, J. Li, X. Zhou, Y. Ni, M. Yu, Y. Zhang, H. Su, Q. Liu and F. Cheng, *J. Am. Chem. Soc.*, 2022, **144**, 11129–11137.

S15 M. Liu, W. Yuan, G. Ma, K. Qiu, X. Nie, Y. Liu, S. Shen and N. Zhang, *Angew. Chem. Int. Ed.*, 2023, **62**, e202304444.

S16 R. Zhang, Y. Feng, Y. Ni, B. Zhong, M. Peng, T. Sun, S. Chen, H. Wang, Z. Tao and K. Zhang, *Angew. Chem. Int. Ed.*, 2023, **62**, e202304503.

S17 X. Yang, C. Li, Z. Sun, S. Yang, Z. Shi, R. Huang, B. Liu, S. Li, Y. Wu, M. Wang, Y. Su, S. Dou and J. Sun, *Adv. Mater.*, 2021, **33**, 2105951.

S18 X. Zeng, K. Xie, S. Liu, S. Zhang, J. Hao, J. Liu, W. Pang, J. Liu, P. Rao, Q. Wang, J. Mao and Z. Guo, *Energy Environ. Sci.*, 2021, **14**, 5947–5957.

S19 J. Zhang, W. Huang, L. Li, C. Chang, K. Yang, L. Gao and X. Pu, *Adv. Mater.*, 2023, **35**, 2300073.

S20 D. Wang, H. Liu, D. Lv, C. Wang, J. Yang and Y. Qian, *Adv. Mater.*, 2022, **35**, 2207908.

S21 S. Jin, P. Chen, Y. Qiu, Z. Zhang, S. Hong, Y. Joo, R. Yang and L. Archer, *J. Am. Chem. Soc.*, 2022, **144**, 19344–19352.

S22 W. Guo, Z. Cong, Z. Guo, C. Chang, X. Liang, Y. Liu, W. Hu and X. Pu, *Energy Storage Mater.*, 2020, **30**, 104–112.

S23 C. Huang, X. Zhao, S. Liu, Y. Hao, Q. Tang, A. Hu, Z. Liu and X. Chen, *Adv. Mater.*, 2021, **33**, 2100445.

S24 J. Dong, H. Peng, J. Wang, C. Wang, D. Wang, N. Wang, W. Fan, X. Jiang, J. Yang and Y. Qian, *Energy Storage Mater.*, 2023, **54**, 875–884.

S25 L. Ma, Q. Li, Y. Ying, F. Ma, S. Chen, Y. Li, H. Huang and C. Zhi, *Adv. Mater.*, 2021, **33**, 200740.

S26 Z. Cai, Y. Ou, B. Zhang, J. Wang, L. Fu, M. Wan, G. Li, W. Wang, L. Wang, J. Jiang, Z. Seh, E. Hu, X. Yang, Y. Cui and Y. Sun, *J. Am. Chem. Soc.*, 2021, **143**, 3143–3152.

S27 X. Yang, C. Li, Z. Sun, S. Yang, Z. Shi, R. Huang, B. Liu, S. Li, Y. Wu, M. Wang, Y. Su, S. Dou and J. Sun, *Adv. Mater.*, 2021, **33**, 2105951.

S28 H. Fan, M. Li and E. Wang, *Nano Energy*, 2022, **103**, 107751.